Int. J. Heat Mass Transfer. Vol. 29, No. 10, pp. 1575–1584, 1986
Printed in Great Britain

0017–9310/86 $3.00+0.00
Pergamon Journals Ltd.

The stability of natural convection in narrow-gap spherical annuli to axisymmetric disturbances

M. T. FARMER, R. W. DOUGLASS† and S. A. TROGDON

255 Walter Scott Engineering Center, Department of Mechanical Engineering, University of Nebraska, Lincoln, NE 68588-0525, U.S.A.

(*Received* 1 *November* 1985 *and in final form* 19 *May* 1986)

Abstract—The linear stability with respect to axisymmetric disturbances of natural convection in narrow-gap, spherical annuli is investigated. The basic motion is an eight-order perturbation solution in the small parameter $\varepsilon = 1-\eta$, where η is the ratio of inner radius of the annulus to outer radius. The disturbance equations are reduced to a system of ordinary differential equations by means of a method of partial spectral expansions. These equations constitute an eigenvalue problem which is solved for the critical Rayleigh number as a function of η and Prandtl number, Pr. Cases considered are $Pr = 0.1$, 1, 10, and 100 for $0.900 \leqslant \eta \leqslant 0.995$. A comparison with the experimental results found in the literature indicates that non-axisymmetric time periodic bifurcation will most likely take precedence over the case considered herein for $Pr = 1, 10$. However, it appears that steady axisymmetric bifurcation is possible for $Pr = 0.1$.

1. INTRODUCTION

STABILITY analyses for a variety of flows in spherical annuli have been reported in the literature. Examples include stability of spherical Couette flows using energy [1] and linear [2] methods, and stability of the motionless state of a thermally stratified fluid, i.e. the spherical analog of the Bénard problem [3–5]. Here, the linear stability of the natural convection-driven basic motion is examined for narrow-gap, spherical annuli. The disturbances are assumed to be axisymmetric. The non-zero basic motion arises through density variations within the fluid due to the inner and outer spherical boundaries being at different temperatures. The density gradient is not everywhere parallel to gravity and thus the fluid is in motion for all non-zero temperature differences across the boundaries. The present investigation is thus to be contrasted with stability analyses for the spherical analog of the Bénard problem.

Motivation for this analysis is provided by the unsteadiness in the basic motion as observed in refs. [6–8] when a certain critical value of the Rayleigh number ($Ra = g\beta\Delta T\Delta R^3/\nu\alpha$) is exceeded. The experiments of Bishop *et al.* [6] and Yin *et al.* [7, 8] have indicated that the nature of the fluid motion is dependent upon the radius ratio and Prandtl number. For Ra below a certain critical value, a steady 'crescent-eddy' (CE) flow pattern is observed in the range of radius ratios ($\eta = R_i/R_o$) of 0.36–0.92 for air as the working fluid (cf. Fig. 1). This flow pattern consists of thin, high speed layers ascending along the inner sphere and descending along the outer sphere with a large, relatively stagnant, central region. As Ra is increased while limiting the radius ratio to small or intermediate values, a steady, kidney-shaped eddy (KSE) flow pattern is observed. The flow is similar to the CE type with the exception that the central low speed region is distorted into a shape resembling a kidney.

If Ra is increased above certain critical values,

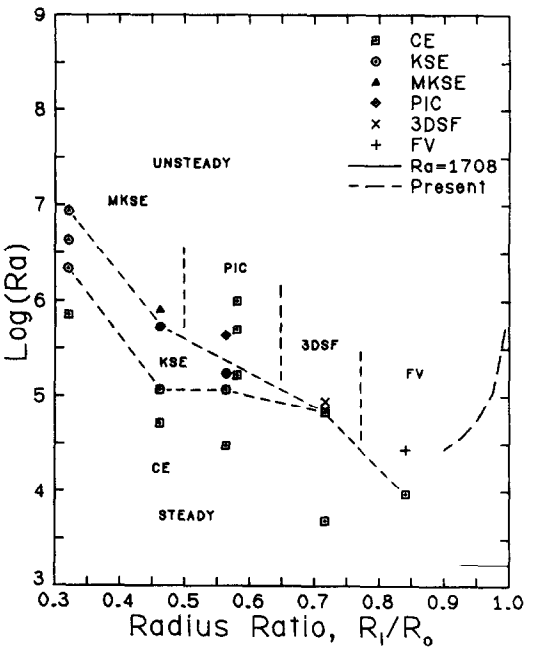

FIG. 1. Natural convection flow regimes for air in spherical annuli based on the flow visualization data of Bishop *et al.* [6] and Yin *et al.* [7, 8]. The results of the present calculations are shown ($Pr = 1$) along with the line $Ra_c = 41.3$ ($\sigma_c = 3.12$) corresponding to the case of a horizontal fluid layer heated from below. The flow regime boundaries are only approximately drawn.

† To whom correspondence should be addressed.

NOMENCLATURE

$\mathbf{e}_r, \mathbf{e}_\theta$	unit vectors in the radial and latitudinal directions, respectively
g	gravitational acceleration constant [m s^{-2}]
$g_n(r)$, $h_n(r)$	partial spectral expansion functions
Gr	Grashof number, $g\beta\Delta T R_o^3/\nu^2$
i	$\sqrt{-1}$
k	thermal conductivity of the fluid [W m^{-1} °C^{-1}]
N_b+1	numbers of terms retained in the base flow expansion
N_d+1	number of terms retained in the disturbance flow expansion
$Nu(\theta)$	local Nusselt number
$\overline{Nu}$	surface-averaged Nusselt number of criticality
P, p	base flow, disturbance pressure field [Pa]
$\hat{P}$	disturbed flow pressure, $P+p\,e^{-st}$ [Pa]
P_n	Legendre polynomial of the first kind of degree n
Pr	Prandtl number, ν/α
r	radial coordinate [m]
r_i^*, r_o^*	inner and outer radii of the spheres, scaled by ΔR
R	stability parameter, $\varepsilon^{3/2}Gr^{1/2}$
Ra	Rayleigh number, $g\beta\Delta T(\Delta R)^3/\nu\alpha$
R_c	value of R at criticality, $Gr_c^{1/2}\varepsilon^{3/2}$
R_i, R_o	inner, outer radius of the spheres [m]
ΔR	R_o-R_i [m]
s	wave number, $\sigma+i\omega$ [s^{-1}]
t	time [s]
T	base flow temperature field [°C]
T_i, T_o	inner, outer surface temperature [°C]
ΔT	T_o-T_i [°C]
v_r, v_θ	radial, latitudinal disturbance velocity [m s^{-1}]
V_r, V_θ	radial, latitudinal base flow velocity [m s^{-1}]
$\hat{\mathbf{v}}$	disturbed flow velocity vector $(\hat{v}_r, \hat{v}_\theta)$ [m s^{-1}].

Greek symbols

α	thermal diffusivity [m^2 s^{-1}]
$\alpha_i, \beta_i, \gamma_i, \delta_i, x_i$	coefficients of the basic motion
β	coefficient of volume expansion [K]
$\Gamma, \Delta, \Xi, \Upsilon, \Omega$	functions describing the base flow
ε	$1-\eta$, relative gap width
ζ	scaled radial coordinate, $(r-\eta)/\varepsilon$
η	radius ratio, T_i/R_o
θ	latitudinal coordinate
ν	kinematic viscosity [m^2 s^{-1}]
ξ	$\cos\theta$
σ	real part of s [s^{-1}]
ϕ	longitudinal coordinate
Φ	disturbance temperature field [°C]
ψ	disturbance streamfunction [m^3 s^{-1}]
Ψ	base flow streamfunction [m^3 s^{-1}]
ω	imaginary part of s [s^{-1}].

Subscript

c	value at criticality.

Superscript

$'$	$d/d\zeta$.

unsteady flows are observed for air. At small radius ratios, the modified kidney-shaped eddy (MKSE) occurs. The pattern is characterized by contractions, of somewhat irregular period, in the central low speed region. At intermediate radius ratios, the periodic interior contraction (PIC) flow regime is reported. This pattern is similar to the MKSE with the exception that the magnitude of the oscillations in the low speed region increase to the point where interaction with the ascending high speed layer occurs. The three-dimensional spiral flow (3DSF) pattern occurs at intermediate to large radius ratios (i.e. $\eta \simeq 1$) and is characterized by the separation of the ascending high speed layer which then shoots into the upper annular region forming counter-rotating vortex pairs. The vortex pairs then become entrained in the descending outer layers forming three-dimensional spiral motions. The falling vortices (FV) flow pattern occurs at large radius ratios and consists of the formation and shedding of counter-rotating cells in the upper annular region. These cells periodically coalesce and then become entrained in the descending flow.

The experimental results for water [7, 8] indicate (cf. Fig. 2) only one steady flow pattern, the steady dog-face type (SDFT), which occurs at all radius ratios for smaller Ra. This pattern consists of three distinct regions. The first is the thin, high speed layers ascending along the inner sphere and descending along the outer sphere. The second is a low speed region which is located in the upper portion of the annulus and is composed of two secondary cells rotating concurrently with the primary flow. In the remainder of the annulus there is a large and relatively stagnant region in which the motion may be detected only by long-time photographic exposures.

As Ra is increased from low values an unsteady dog-face type (USDFT) flow develops which is similar to the SDFT with the exception that the upper secondary cell is no longer stationary. The cell randomly forms and then submerges itself in the large stagnant region

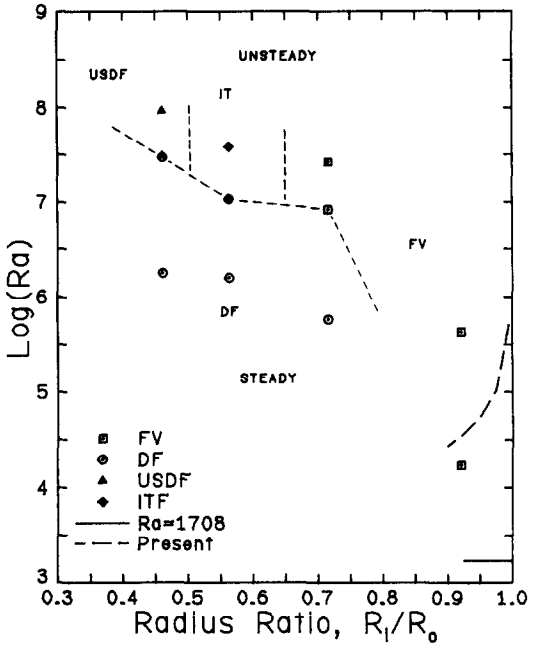

FIG. 2. Natural convection flow regimes for water in spherical annuli [7, 8]. Results from the present calculations with $Pr = 10$ are shown. The line $Ra_c = 41.3$ ($\sigma_c = 3.12$) corresponding to the case of a horizontal fluid layer heated from below is also shown. The flow regime boundaries are only approximately drawn.

occupying the upper annular region. Other unsteady flow patterns for water include the interior tertiary (IT) flow pattern which occurs at intermediate radius ratios with sufficiently large Ra. In this flow, the weak shear region between the secondary cells of the SDFT flow expand to form a weak, oscillatory, tertiary cell while the upper secondary cell is reduced in size. At large radius ratios, a FV flow pattern is observed which is similar to the FV flows for air.

Aside from the flow visualization results, many analytical and numerical studies have been conducted to determine the basic motion in this geometry. The majority of these studies use the steady form of the governing equations (e.g. [9–11]) although some have used the transient formulation (e.g. [12, 13]). Only one work, that of Robertson [13], actually reported evolutionary results. In general, the computed steady streamline contours and isotherms show good agreement with the flow visualization results, especially for air. None of these studies report transition to unsteady flow for increasing Ra, as was observed in the flow visualization experiments.

Analytical studies of the stability of natural convection in spherical annuli is, to the best of our knowledge, non-existent in the literature. In a related geometry, Mojtabi *et al.* [14] used the energy stability theory to perform a local analysis of the stability of natural convection in concentric, cylindrical annuli. The base flow was calculated by a perturbation method in Rayleigh number and terms were maintained through second order. The temperature and radial velocity disturbances were developed as periodic wave functions of the axial coordinate. Results of their analysis indicate that as $\eta \to 1$, the critical Rayleigh number tends to 1708 with a wave number of 3.12, corresponding to the onset of convection in a horizontal fluid layer with rigid–rigid boundaries and heated from below [15].

In the present study, linear theory is used to examine the stability with respect to axisymmetric disturbances of natural convection in a narrow-gap, spherical annulus with isothermal boundaries. Specifically, the objective is to find a first approximation to the dividing line between steady and unsteady flows for $\eta \simeq 1$ as reported in the experimental studies [6–8].

2. THE BASIC MOTION

An approximate closed form solution for the flow in this geometry has been obtained by Wright [10] for the special case of narrow-gap, spherical annuli. This solution is briefly described here.

The physical domain is bounded by concentric inner and outer spherical surfaces of radii R_i and R_o which are maintained at uniform temperatures T_i and T_o, respectively, with $T_i > T_o$. Standard spherical coordinates are used with (r, ξ, ϕ) being the dimensionless radius, cosine of the polar angle θ, and azimuthal angle, respectively. The fluid is assumed to be strictly Boussinesq and the motion is assumed to be axisymmetric. Taking the curl of the momentum equation and introducing a streamfunction defined in terms of V_r and V_θ as

$$V_r = -\frac{1}{r^2}\frac{\partial \Psi}{\partial \xi}, \quad V_\theta = -\frac{(1-\xi^2)^{-1/2}}{r}\frac{\partial \Psi}{\partial r} \tag{1}$$

it is found that the momentum and energy equations become

$$E^4\Psi = Gr^{1/2}\left\{\frac{(1-\xi^2)}{r^2}\frac{\partial}{\partial \xi}\left[\frac{E^2\Psi}{(1-\xi^2)}\frac{\partial \Psi}{\partial r}\right] - \frac{\partial}{\partial r}\left[\frac{E^2\Psi}{r^2}\frac{\partial \Psi}{\partial \xi}\right] - (1-\xi^2)\left[r\frac{\partial T}{\partial r} - \xi\frac{\partial T}{\partial \xi}\right]\right\} \tag{2}$$

$$\nabla^2 T = \frac{PrGr^{1/2}}{r^2}\left[\frac{\partial \Psi}{\partial r}\frac{\partial T}{\partial \xi} - \frac{\partial \Psi}{\partial \xi}\frac{\partial T}{\partial r}\right] \tag{3}$$

where

$$E^2(\cdot) = \frac{\partial^2(\cdot)}{\partial r^2} + \frac{(1-\xi^2)}{r^2}\frac{\partial^2(\cdot)}{\partial \xi^2}$$

$$\nabla^2(\cdot) = \frac{1}{r^2}\frac{\partial}{\partial r}\left[r^2\frac{\partial(\cdot)}{\partial r}\right] + \frac{1}{r^2}\frac{\partial}{\partial \xi}\left[(1-\xi^2)\frac{\partial}{\partial \xi}(\cdot)\right].$$

In (2) and (3), Ψ has been scaled in terms of the fluid particle buoyancy rise velocity, T in terms of the temperature difference across the gap, and r in terms of R_o. The Prandtl and Grashof numbers are defined,

respectively, as

$$Pr = \frac{\nu}{\alpha}, \quad Gr = g\beta\Delta T R_o^3/\nu^2.$$

The four boundary conditions on Ψ and the two boundary conditions on T are obtained from the no-slip and constant temperature conditions at the inner and outer boundaries. Hence

$$\frac{\partial\Psi}{\partial r}(\eta,\xi) = \frac{\partial\Psi}{\partial r}(1,\xi) = \frac{\partial\Psi}{\partial\xi}(\eta,\xi) = \frac{\partial\Psi}{\partial\xi}(1,\xi) = 0 \quad (4)$$

$$T(\eta,\xi) = 1, \quad T(1,\xi) = 0 \quad (5)$$

where $\eta = R_i/R_o$.

Wright examined the case of narrow annular gaps, which in terms of η requires $1-\eta = \varepsilon \ll 1$. To indicate explicitly the relative order-of-magnitude of terms for this case, the radial coordinate r in (2) and (3) was rescaled in terms of the dimensionless variable ζ as

$$\zeta = \frac{r-\eta}{\varepsilon} \quad (6)$$

so that the radial coordinate is mapped onto ζ: [0, 1]. Wright found that under this scaling (2) and (3) with (4) and (5) admitted a perturbation solution in ε of the form

$$\Psi(\zeta,\xi) \simeq \sum_{n=0}^{N_b} \varepsilon^n \Psi_n(\zeta,\xi) \quad (7)$$

$$T(\zeta,\xi) \simeq \sum_{n=0}^{N_b} \varepsilon^n T_n(\zeta,\xi). \quad (8)$$

Substituting (7) and (8) into (2) and (3), Wright found that for a given order of ε, the problem was reduced to one of solving ordinary differential equations in Ψ_n and T_n with only derivatives with respect to ζ occurring on the LHS. Closed form solutions were obtained through $N_b = 8$ and in tabular form through $N_b = 11$.

In the solution of the stability problem it was found that the numerical technique used to solve the equations was somewhat better behaved when the equations were rescaled in terms of the gap width, $\Delta R = R_o - R_i$, as the length scale. In terms of this scaling, Wright's solution may be expressed as

$$\Psi(\zeta,\xi) \simeq (1-\xi^2)[\Gamma(\zeta; R, Pr, \varepsilon) + \xi\Delta(\zeta; R, Pr, \varepsilon)] \quad (9)$$

$$T(\zeta,\xi) \simeq \Upsilon(\zeta; R, Pr, \varepsilon) + \xi[\Xi(\zeta; R, Pr, \varepsilon) + \xi\Omega(\zeta; R, Pr, \varepsilon)] \quad (10)$$

where

$$\Gamma = \frac{R}{\varepsilon^4}\sum_{i=2}^{9}(-1)^i\alpha_i\zeta^i$$

$$\Delta = \frac{R^3}{\varepsilon^7}\sum_{i=2}^{10}(-1)^i\beta_i\zeta^i$$

$$\Upsilon = 1 + \sum_{i=1}^{11}(-1)^i\gamma_i\zeta^i \quad (11)$$

$$\Xi = \frac{R^2 Pr}{\varepsilon^3}\sum_{i=1}^{10}(-1)^i\delta_i\zeta^i$$

and

$$\Omega = \varepsilon^2 R^4 Pr \sum_{i=1}^{11}(-1)^i\chi_i\zeta^i.$$

In (9) and (10), r is now scaled in terms of the gap width. The parameter R is the square root of the Grashof number based on gap width

$$R = \left[\frac{g\beta\Delta T\Delta R^3}{\nu^2}\right]^{1/2} = \varepsilon^{3/2}Gr^{1/2}. \quad (12)$$

The coefficients α_i, β_i, γ_i, δ_i and χ_i in (12) are continuous functions of R, Pr and ε. The coefficients are quite lengthy and are omitted here; they can be found in ref. [16]. Information on the range of applicability and convergence of (9) and (10) can be found in ref. [10].

3. THE STABILITY PROBLEM

We begin by writing the equations of motion governing the time evolution of the flow for a Boussinesq fluid in spherical coordinates. When the length scale is based on ΔR the variable r is replaced by $r\varepsilon$, and we find with $\zeta = r - \eta/\varepsilon$ that

$$\nabla\cdot\hat{\mathbf{v}} = 0 \quad (13)$$

$$\frac{\partial}{\partial t}\hat{\mathbf{v}} + R\hat{\mathbf{v}}\cdot\nabla\hat{\mathbf{v}} = -\nabla\hat{P} + R\hat{T}(\xi\mathbf{e}_r - (1-\xi^2)^{1/2}\mathbf{e}_\theta) + \nabla^2\hat{\mathbf{v}} \quad (14)$$

$$Pr\frac{\partial\hat{T}}{\partial t} + PrR\hat{\mathbf{v}}\cdot\nabla\hat{T} = \nabla^2\hat{T}. \quad (15)$$

The dependent variables are now decomposed into a component representing the basic motion and a component representing a perturbation of the basic motion. It is assumed that the disturbances are *axisymmetric* and that the solutions to the perturbation quantities are in terms of exponentials. The dependent variables are written as

$$\hat{\mathbf{v}}(r,\xi,t) = \mathbf{V}(r,\xi) + \mathbf{v}(r,\xi)\,e^{-st} \quad (16)$$

$$\hat{T}(r,\xi,t) = T(r,\xi) + \Phi(r,\xi)\,e^{-st} \quad (17)$$

$$\hat{P}(r,\xi,t) = P(r,\xi) + p(r,\xi)\,e^{-st} \quad (18)$$

where $s = \sigma + i\omega$; $\mathbf{V}$, P and T are basic motion quantities, and v, p and Φ are disturbance quantities. Equations (16)–(18) are now substituted into (13)–(15) and nonlinear terms in the disturbance quantities are neglected. Taking the curl of (14) and introducing basic motion and disturbance streamfunctions Ψ and ψ, respectively, (14) and (15) become

$$E^4\psi + sE^2\psi = R\left\{\frac{(1-\xi^2)}{r^2}\frac{\partial}{\partial\xi}\times\left[\frac{E^2\Psi}{(1-\xi^2)}\frac{\partial\psi}{\partial r} + \frac{\partial\Psi}{\partial r}\frac{E^2\psi}{(1-\xi^2)}\right] - \frac{\partial}{\partial r}\left[\frac{\partial\Psi}{\partial\xi}\frac{E^2\psi}{r^2} + \frac{E^2\Psi}{r^2}\frac{\partial\psi}{\partial\xi}\right] - (1-\xi^2)\left[r\frac{\partial\Phi}{\partial r} - \xi\frac{\partial\Phi}{\partial\xi}\right]\right\} \quad (19)$$

$$\nabla^2\Phi + Prs\Phi = \frac{PrR}{r^2}\left[\frac{\partial\Psi}{\partial r}\frac{\partial\Phi}{\partial\xi} - \frac{\partial\Psi}{\partial\xi}\frac{\partial\Phi}{\partial r} + \frac{\partial T}{\partial\xi}\frac{\partial\psi}{\partial r} - \frac{\partial T}{\partial r}\frac{\partial\psi}{\partial\xi}\right]. \quad (20)$$

From (4) and (5) and (16) and (17) one finds that the conditions on ψ and Φ are

$$\frac{\partial\psi}{\partial r}(r_i^*,\xi) = \frac{\partial\psi}{\partial r}(r_o^*,\xi) = \frac{\partial\psi}{\partial\xi}(r_i^*,\xi) = \frac{\partial\psi}{\partial\xi}(r_o^*,\xi) = 0 \quad (21)$$

$$\Phi(r_i^*,\xi) = \Phi(r_o^*,\xi) = 0 \quad (22)$$

where, under the scaling based on gap width, $r_i^* = \eta/\varepsilon$ and $r_o^* = 1/\varepsilon$. Equations (19) and (20) with (21) and (22) compose the eigenvalue problem governing the linear stability of (9) and (10) to axisymmetric disturbances.

To reduce the system of partial differential equations to a system of ordinary differential equations, the method of partial spectral expansions is used. The dependent variables are therefore expressed as

$$\psi(r,\xi) \simeq (1-\xi^2)\sum_{n=0}^{N_d} g_n(r)P_n(\xi) \quad (23)$$

$$\Phi(r,\xi) \simeq \sum_{n=0}^{N_d} h_n(r)P_n(\xi) \quad (24)$$

where $P_n(\xi)$ are the Legendre polynomials of the first kind of degree n and $g_n(r)$ and $h_n(r)$, $n = 0, 1, \ldots, N_d$, are to-be-determined functions of r. Note that the term $(1-\xi^2) = \sin^2\theta$ has been introduced in (23) to ensure the condition of no flow across the polar axis, consistent with the assumption of axisymmetric disturbances. One can easily verify that the analogous insulated condition for Φ is identically satisfied by (24) at $\xi = -1, 1$.

To eliminate the angular dependence, (9) and (10) and (23) and (24) are substituted into (19) and (20). The resultant equations are then multiplied by $P_m(\xi)$, where m ranges from $0 \leqslant m \leqslant N_d$, and then integrated over the domain $\xi: [-1, 1]$. Using the orthogonality and recursion relationship for the Legendre polynomials, the explicit angular dependence can then be eliminated. Evaluation of these integrals results in coefficient matrices indexed by m and n. For each index $m, 0 \leqslant m \leqslant N_d$, the following equations are then obtained.

$$g_m'''' = -\frac{R\Delta}{r^2}g_m''' + \left\{\frac{2m(m+1)+2}{r^2} - s + \frac{2R\Delta}{r^3}\right\}g_m'' + \left\{R\left[\frac{\Delta''}{r^2} - \frac{6\Delta}{r^4}\right] - \frac{4[m(m+1)+2]}{r^3} + \frac{R\Delta[m(m+1)+2]}{r^4}\right\}g_m'$$
$$+ \left\{\frac{8-m(m+1)[m(m+1)+2]}{r^4} + \frac{s[m(m+1)+2]}{r^2} - \frac{4R\Delta[m(m+1)+2]}{r^5}\right\}g_m$$
$$- rRh_m' + \frac{R(2m+1)}{2}\sum_{n=0}^{N_d}\{A_{mn}g_n + B_{mn}g_n' + C_{mn}g_n'' + D_{mn}g_m''' + E_{mn}h_n\} \quad (25)$$

$$h_m'' = -\frac{2}{r}h_m' + \frac{[m(m+1) - Prsr^2]}{r^2}h_m + \frac{PrR}{r^2}(\Xi g_m' - \Delta h_m') + \frac{PrR(2m+1)}{2} \times \sum_{n=0}^{N_d}\{F_{mn}h_n + G_{mn}h_n' + H_{mn}g_n + I_{mn}g_n'\} \quad (26)$$

where $' \equiv \mathrm{d}/\mathrm{d}r$. In (25) and (26), the radially-dependent base flow functions have been evaluated at $\zeta = \zeta(r)$.

The coefficients $A_{mn}, B_{mn}, \ldots, I_{mn}$ under the summation signs in (25) and (26) contain the base flow functions (11) as well as the coefficient matrices arising from the Legendre polynomial integrals. The expressions for these coefficients and coefficient matrices are quite lengthy and are given in the Appendix.

From (21)–(24), it is easily shown that boundary conditions on the unknown functions $g_n(r)$ and $h_n(r)$ are

$$g_n(r_i^*) = g_n'(r_i^*) = g_n(r_o^*) = g_n'(r_o^*) = 0, \quad n = 0, 1, \ldots, N_d \quad (27)$$

$$h_n(r_i^*) = h_n(r_o^*) = 0, \quad n = 0, 1, \ldots, N_d. \quad (28)$$

To solve (25) and (26) with (27) and (28), we assume that a principle of exchange of stability exists. Hence, s is set to zero in (25) and (26) and R is treated as the stability parameter. The lowest value of R for which (25) and (26) with (27) and (28) admits a nontrivial solution is then the critical Grashof number, R_c^2.

The equations are solved by forward integration using the classic fourth-order Runge–Kutta [17] technique. The numerical scheme is similar to that reported by ref. [2]. A brief description is provided here; full details can be found in ref. [16].

Equations (25) and (26) with conditions (27) and (28) is in the form of a boundary value problem. To solve via forward integration, one is then confronted with $3N_d+3$ unknown conditions at either boundary. To circumvent this, define $3N_d+3$ sets of $3N_d+3$ linearly independent 'guessed' conditions at (say) r_i^*. Equations (25) and (26) are then integrated once for each set of extra conditions in conjunction with the known conditions (27) and (28), thus requiring $3N_d+3$ integrations of the governing equations. The values of the dependent variables g_n, g_n' and $h_n, n = 0, 1, \ldots, N_d$, will in general not meet the required conditions (27) and (28). However, the problem is linear so that a

linear combination of the independent solutions can be constructed which meet the required conditions. For the problem to have a nontrivial solution, the determinant of the coefficient matrix of the linear combination of the solutions must vanish when evaluated at r_o^*. In general, this condition cannot be met for arbitrary values of R. Hence, R is increased from zero until the determinant changes sign. This criterion then determines the value of the critical Grashof number, R_c^2.

In terms of numerical accuracy, the number of integration steps was varied to determine the number required to reduce changes in R_c to less than 0.10%. It was found that 20 integration steps were sufficient for all combinations of η and Pr considered.

4. RESULTS AND DISCUSSION

The computer algorithm was designed to calculate R_c for given values of the parameters η, Pr, N_b and N_d. For the computations, N_b was fixed at eight and N_d was varied from 0 to 12 to ascertain the converged value of R_c for given η and Pr. Fluids with Prandtl numbers of 0.1, 1.0, 10 and 100 were considered for radius ratios ranging from 0.900 to 0.995, i.e. $\varepsilon = 0.005$–0.1.

The convergence of R_c with increasing N_d was found to be oscillatory. Figures 3 and 4 illustrate the nature of the convergence for the two cases $Pr = 1$ with $\eta = 0.950$ and $Pr = 10$ for $\eta = 0.995$. The series clearly converged only for the cases $Pr = 10$ and 100 for $\eta = 0.995$. The epsilon algorithm [18], a sequential method for calculating Padé approximates, was used to estimate the converged value of R_c. It was determined that the nature of the convergence to R_c became apparent after $N_d = 1$; therefore, the epsilon algorithm was applied to the partial sums from $N_d = 2$–12. The results of the epsilon algorithm calculations are indicated in Figs. 3 and 4.

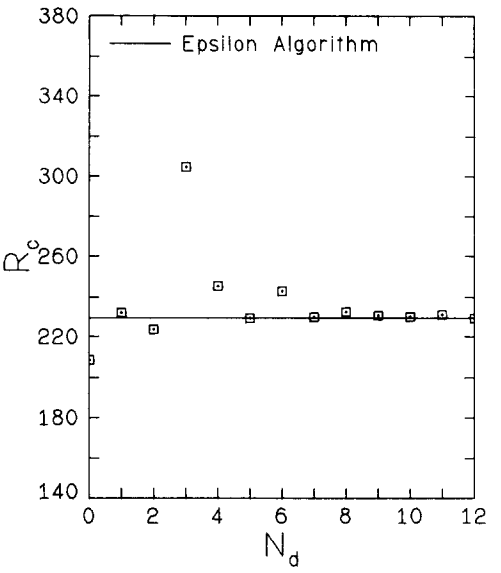

FIG. 4. The influence of the number of terms retained in the partial spectral expansion on R_c for the disturbance flow field. In this case, $Pr = 10$ and $\eta = 0.995$. The convergent value of R_c was predicted from the epsilon algorithm [18].

Figure 5 shows the critical Rayleigh number results for the various Prandtl numbers considered. In terms of the stability parameter R, the Rayleigh number based on gap width is

$$Ra = R^2 Pr \tag{29}$$

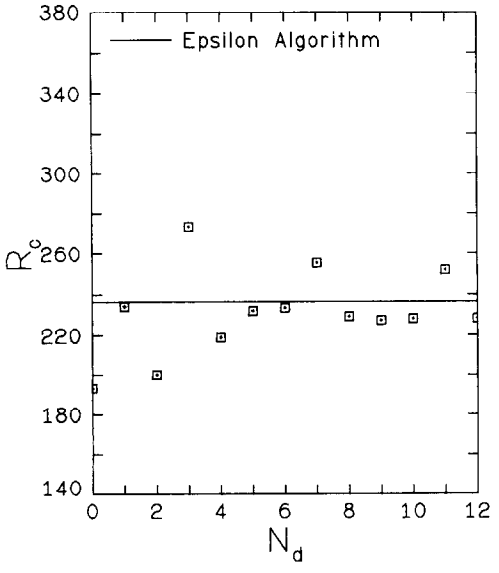

FIG. 3. The influence of the number of terms retained in the partial spectral expansion on R_c for the disturbance flow field. In this case, $Pr = 1$ and $\eta = 0.950$. The convergent value of R_c was predicted from the epsilon algorithm [18].

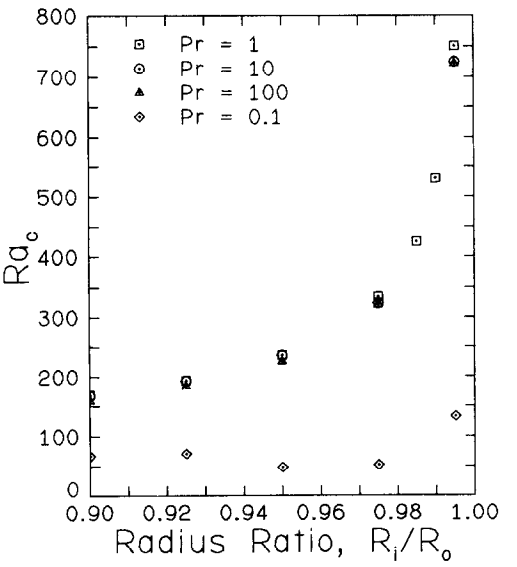

FIG. 5. A summary of the critical Rayleigh numbers for natural convection in narrow-gap, spherical annuli with axisymmetric disturbances is shown in this illustration.

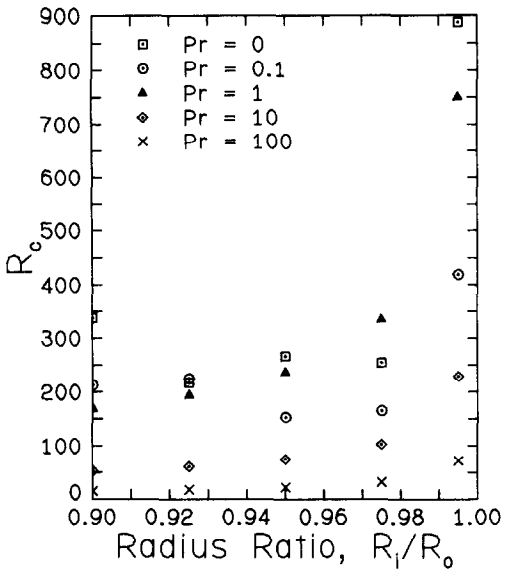

FIG. 6. The dependence of the stability parameter $R_c = Ra_c/Pr^{1/2}$ on the Prandtl number is shown using the data of Fig. 5. In addition, data for the limiting case $Pr = 0$ are included. R_c does not include the Prandtl number in its definition.

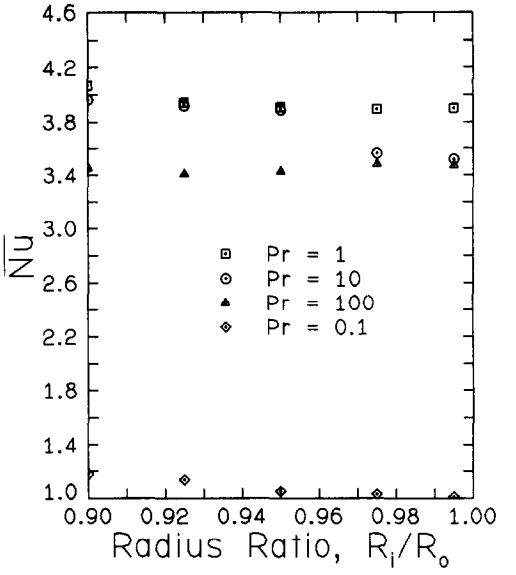

FIG. 7. The dimensionless average surface heat transfer rate, $\overline{Nu}$, at criticality is shown.

and shown in Fig. 5 is

$$Ra_c = R_c Pr^{1/2}. \tag{30}$$

Figure 5 indicates that for Prandtl numbers of 1, 10 and 100, the data appear to coalesce into a single curve when plotted in terms of Ra_c. For $Pr = 0.10$, however, the data lie significantly below the trend set by the remainder of the data. This occurrence indicates that the Rayleigh number cannot be used as a single parameter to determine instability. That this is true may be illustrated by the following argument. One would like to look at the limiting case $Pr \to 0$. No-slip boundary conditions have been imposed; thus, to take this limit, one must consider the case $\alpha \to \infty$ with ν finite since $Pr = \nu/\alpha$. Then, for $Pr \to 0$, the disturbance energy equation (26) corresponds to Laplace's equations in spherical coordinates and since the boundary conditions on Φ are homogeneous, the only solution is $\Phi = 0$. The disturbance problem then becomes strictly hydrodynamic. The case $\alpha \to \infty$ with ΔT finite implies $Ra \to 0$. Hence, in the limit $Pr \to 0$, it appears that the Grashof number rather than the Rayleigh number should be viewed as the parameter controlling stability. Indeed, as $Pr \to 0$, the base state temperature solution (10) approaches the conduction solution and the streamfunction solution (9) becomes solely dependent upon the Grashof number, i.e. $\Psi(R, Pr, \varepsilon) \to \Psi(R, \varepsilon)|_{Pr \to 0}$. The results of Fig. 5 have been replotted in Fig. 6 in terms of $R_c = Ra_c/Pr^{1/2}$ (numerical values are listed in Table 1) in order to illustrate the dependence of R_c on Pr as the limit $Pr = 0$ is approached.

Figure 7 is a plot of the average Nusselt number, $\overline{Nu}$, at the critical point for the different Prandtl number fluids considered. $\overline{Nu}$ is defined to be the integrated average of the local Nusselt number over the inner spherical surface. The local Nusselt number is taken to be the ratio of the local heat transfer rate to a reference rate defined to be

$$q_r = -k\frac{\Delta T}{\Delta R}. \tag{31}$$

Upon evaluation of the integral, one finds

$$\overline{Nu} = -\{\Gamma'(r_i^*) + \tfrac{1}{3}\Omega'(r_i^*)\} \tag{32}$$

where Γ and Ω are defined under (11). Figure 7

Table 1. Values of the stability parameter, R_c

	Pr				
η	0.0	0.1	1.0	10.0	100.0
0.900	338.0	213.1	168.7	52.9	15.9
0.925	217.3	224.8	193.9	61.0	18.4
0.950	266.6	152.6	236.6	74.7	22.6
0.975	254.6	164.5	334.8	102.7	32.2
0.985	—	—	424.4	—	—
0.990	—	—	530.2	—	—
0.995	887.6	419.8	750.5	229.2	72.2

indicates that $\overline{Nu}$ is relatively insensitive to η. There are slight fluctuations, but this is believed to be a result of inaccurate predictions of the converged value of R_c using the epsilon algorithm.

The present results are compared with the experimental flow visualization results of Bishop *et al.* [6] and Yin *et al.* [7, 8] in Figs. 1 and 2. In these figures we have delineated (to the best of our ability to interpret the data) the various reported flow regimes, including the regions of steady and unsteady flows. Also included is the result $Ra_c = 41.3$ with wave number 3.12 for the case of a horizontal fluid layer heated from below with rigid–rigid boundaries. Mojtabi *et al.* [14] also found these to be the associated limiting values for the case of horizontal, coaxial cylinders.

The present results for air and water indicate that $Ra_c \to \infty$ as $\eta \to 1$, in agreement with the results of the Bénard problem [15] with wave number 0 (i.e. axisymmetric disturbances). The experimental data [6–8] would seem to indicate that the transition line between steady and unsteady flows approaches $Ra_c = 41.3$ as $\eta \to 1$ and also that the nature of the bifurcated flow for large η is three-dimensional and time periodic (i.e. the FV flow pattern). The present results assume, *a priori*, the existence of steady bifurcating solutions and therefore the analysis fails in predicting this transition. However, the results of the current work will provide an upper bound to the critical Rayleigh number.

There is presently no experimental data for which a comparison with the $Pr = 100$ and 0.10 results can be made. The results for $Pr = 0.10$ indicate that the possibility for steady axisymmetric bifurcation at large η does exist. The conclusion is drawn from Fig. 7, where it is seen that the heat transport rates are exceedingly low at the critical point.

5. CONCLUSION

The linear stability of natural convection in narrow-gap, spherical annuli has been investigated. A comparison with the experimental data found in the literature indicates that non-axisymmetric, time periodic bifurcation will most likely take precedence over the case considered herein for fluids with $Pr = 1, 10$. For $Pr = 0.10$, the results indicate the possibility of steady, axisymmetric, bifurcated solutions.

Acknowledgements—The authors would like to thank Mr David Gardner for his assistance in computing the $Pr = 0$ results. In addition, thanks are expressed to the College of Engineering and Technology of the University of Nebraska which supplied computational support for this research effort.

REFERENCES

1. B. R. Munson and D. D. Joseph, Viscous incompressible flow between concentric rotating spheres. Part 2. Hydrodynamic stability, *J. Fluid Mech.* **49**, 305–318 (1971).
2. B. R. Munson and M. Menguturk, Viscous incompressible flow between concentric rotating spheres. Part 3. Linear stability and experiments, *J. Fluid Mech.* **69**, 705–719 (1975).
3. F. H. Busse, Patterns of convection in spherical shells, *J. Fluid Mech.* **72**, 65–85 (1975).
4. F. H. Busse and N. Riahi, Patterns of convection in spherical shells. Part 2, *J. Fluid Mech.* **123**, 283–301 (1982).
5. P. Chossat and J. P. Girard, Calcul des coefficients de bifurcation dans un problème de convection en symétrie sphérique, *J. Méc. theor. appl.* **2**, 799–828 (1983).
6. E. H. Bishop, R. S. Kolfat, L. R. Mack and J. A. Scanlan, Convective heat transfer between concentric spheres, *Proc. 1964 Heat Transfer and Fluid Mechanics Institute*, pp. 69–80. Stanford University Press, Stanford, CA (1964).
7. S. H. Yin, Natural convective flow between isothermal concentric spheres. Ph.D. dissertation, Montana State University, Bozeman, MT (1972).
8. S. H. Yin, R. E. Powe, J. A. Scanlan and E. H. Bishop, Natural convection flow patterns in spherical annuli, *Int. J. Heat Mass Transfer* **16**, 1785–1795 (1973).
9. H. C. Hardee, Natural convection between concentric spheres at low Rayleigh numbers. Ph.D. dissertation, University of Texas, Austin, TX (1966).
10. J. L. Wright and R. W. Douglass, Natural convection in narrow-gap spherical annuli, *Int. J. Heat Mass Transfer* **29**, 725–739 (1986); or J. L. Wright, Natural convective flow in narrow gap spherical annuli. M.S. thesis, University of Nebraska—Lincoln (1984).
11. J. Ebert, Computation of free convection in heated enclosures. M.S. thesis, University of Oklahoma (1984).
12. I. G. Sevruk, Transient heat convection within a spherical film, *P.M.M.* (*J. appl. Math. Mech.*) **22**, 419–423 (1958).
13. S. J. Robertson, Numerical simulation of natural convection in a spherical container due to cooling at the center (idealization of Lal–Kroes experiment), NASA-CR-163955, Lockheed Missiles and Aircraft Co., Huntsville Research and Engineering Center, Huntsville, AL (1981).
14. A. Mojtabi and J.-P. Caltagirone, Energy stability of a natural convective flow in a horizontal annular space, *Phys. Fluids* **22**, 1208–1209 (1979).
15. S. Chandrasekhar, *Hydrodynamic and Hydromagnetic Stability*. Oxford University Press, Oxford (1961).
16. M. T. Farmer, Stability of natural convection in a spherical annulus to axisymmetric disturbances. M.S. thesis, University of Nebraska—Lincoln (1985).
17. M. L. James, G. M. Smith and J. C. Wolford, *Applied Numerical Methods for Digital Computations*. Harper & Row, New York (1977).
18. J. R. MacDonald, Accelerated convergence, divergence, iteration, extrapolation, and curve fitting, *J. appl. Phys.* **35** (1964).

APPENDIX

The following expressions are the coefficients which appear in the disturbance equations (25) and (26). The quantities $CI(m,n)$, $I = 1, 2, \ldots, 8$ in the coefficients are a result of the orthogonalization procedure and are defined in the latter part of the Appendix

$$A_{mn} = \left\{\frac{2\sigma r^2 - 4[n(n+1)-2]}{r^4 R} - \frac{32\Delta}{r^5} - \frac{[n(n+1)-2]\Delta'}{r^4} - \left(\frac{\Delta''}{r^2}\right)'\right\} C1(m,n) + \left\{\frac{8[n(n+1)+4]\Gamma}{r^5}\right.$$

$$+\frac{2[n(n+1)-2]\Gamma'}{r^4}+2\left(\frac{\Gamma''}{r^2}\right)'\Bigg\}C2(m,n)$$
$$+\left\{\frac{12[n(n+1)+6]\Delta}{r^5}+\frac{2[n(n+1)-6]\Delta'}{r^4}\right.$$
$$\left.+2\left(\frac{\Delta''}{r^2}\right)'\right\}C3(m,n)-\left\{\frac{8\Gamma}{r^5}+\frac{[n(n+1)+2]\Gamma'}{r^4}\right.$$
$$\left.-\left(\frac{\Gamma''}{r^2}\right)'\right\}C4(m,n)+\left\{\frac{24\Gamma}{r^5}+\frac{[n(n+1)-2]\Gamma'}{r^4}\right.$$
$$\left.+\left(\frac{\Gamma''}{r^2}\right)'\right\}C5(m,n)+\left\{\frac{48\Delta}{r^5}+\frac{[n(n+1)-6]\Delta'}{r^4}\right.$$
$$\left.+\left(\frac{\Delta''}{r^2}\right)'\right\}C6(m,n)$$

$$B_{mn}=\left[\frac{2\Delta}{r^4}-\frac{8}{r^3R}\right]C1(m,n)-\frac{2[n(n+1)+2]\Gamma C2(m,n)}{r^4}$$
$$-\left\{\frac{3n(n+1)\Delta}{r^4}+\frac{\Delta''}{r^2}\right\}C3(m,n)-\frac{4\Gamma C5(m,n)}{r^4}$$
$$-\frac{6\Delta C6(m,n)}{r^4}$$

$$C_{mn}=\left[\frac{4}{r^2R}+\frac{\Delta'}{r^2}\right]C1(m,n)-\frac{4\Gamma C2(m,n)}{r^3}-\frac{6\Delta C3(m,n)}{r^3}$$
$$+\frac{\Gamma'[C4(m,n)-C5(m,n)]}{r^2}-\frac{\Delta' C6(m,n)}{r^2}$$

$$D_{mn}=\frac{[2\Gamma C2(m,n)+3\Delta C3(m,n)]}{r^2}$$

$$E_{mn}=C1(m,n)$$

$$F_{mn}=\Gamma'[C4(m,n)-C5(m,n)]+\Delta'[C1(m,n)-C6(m,n)]$$

$$G_{mn}=2\Gamma C2(m,n)+3\Delta C3(m,n)$$

$$H_{mn}=\Upsilon'[C5(m,n)-C4(m,n)+2C2(m,n)]$$
$$+\Xi'[C6(m,n)-C1(m,n)+2C3(m,n)]$$
$$+\Omega'[C7(m,n)-C5(m,n)+2C8(m,n)]$$

$$I_{mn}=2\Omega[C2(m,n)-C8(m,n)]-\Xi C3(m,n)$$

$$C1(m,n)=\langle\xi P_n',P_m\rangle$$
$$C2(m,n)=\langle\xi P_n,P_m\rangle$$
$$C3(m,n)=\langle\xi^2P_n,P_m\rangle$$
$$C4(m,n)=\langle P_n',P_m\rangle$$
$$C5(m,n)=\langle\xi^2P_n',P_m\rangle$$
$$C6(m,n)=\langle\xi^3P_n',P_m\rangle$$
$$C7(m,n)=\langle\xi^4P_n',P_m\rangle$$
$$C8(m,n)=\langle\xi^3P_n,P_m\rangle$$

where:

$$\langle(\cdot),P_m\rangle=\int_{-1}^{+1}(\cdot)P_m\,d\xi$$

$$C1(m,n)=\begin{cases}\dfrac{2n}{2n+1}, & n=m\\ 1+(-1)^{n+m}, & n>m\\ 0, & \text{otherwise}\end{cases}$$

$$C2(m,n)=\begin{cases}\dfrac{2(n+1)}{(2n+1)(2n+3)}, & m=n+1\\ \dfrac{2n}{(2n+1)(2n-1)}, & m=n-1\\ 0, & \text{otherwise}\end{cases}$$

$$C3(m,n)=\begin{cases}\dfrac{(n+1)(n+2)}{(n+\frac{1}{2})(2n+3)(2n+5)}, & m=n+2\\ \dfrac{n(n-1)}{(n+\frac{1}{2})(2n-1)(2n-3)}, & n=m+2\\ \dfrac{(n+1)^2}{(2n+1)^2(n+\frac{3}{2})}+\dfrac{n^2}{(2n+1)^2(n-\frac{1}{2})}, & m=0\\ 0, & \text{otherwise}\end{cases}$$

$$C4(m,n)=\begin{cases}2, & n=m+1\\ 1-(-1)^{n+m}, & n>m+1\\ 0, & \text{otherwise}\end{cases}$$

$$C5(m,n)=\begin{cases}\dfrac{(2n+1)(2n-1)-n(n+1)}{(n+\frac{1}{2})(2n-1)}, & n=m+1\\ 1-(-1)^{n+m}, & n>m+1\\ \dfrac{n(n+1)}{(n+\frac{1}{2})(2n+3)}, & n=m-1\\ 0, & \text{otherwise}\end{cases}$$

$$C6(m,n)=\begin{cases}\dfrac{n}{(n+\frac{1}{2})}+\dfrac{n(n+1)^2}{(2n+1)^2(n+\frac{3}{2})}-\dfrac{n^2(n+1)}{(2n+1)^2(n-\frac{1}{2})}, & m=n\\ \dfrac{n(n+1)(n+2)}{(n+\frac{1}{2})(2n+3)(2n+5)}, & n=m-2\\ 2+\dfrac{n(1-n)(n+1)}{(n+\frac{1}{2})(2n-1)(2n-3)}, & n=m+2\\ 1+(-1)^{n+m}, & n>m \text{ and } n\neq m+2\\ 0, & \text{otherwise}\end{cases}$$

$$C7(m,n)=\begin{cases}2+\dfrac{n(n+1)}{(n+\frac{1}{2})(2n-1)}\left[\dfrac{n(n+1)}{(2n+1)(2n+3)}-\dfrac{(n-1)^2+(2n-1)(2n-3)}{(2n-1)(2n-3)}-\dfrac{n^2}{(2n-1)(2n+1)}\right], & m=n-1\\ \dfrac{n(n+1)}{(2n+3)}\left[\dfrac{1}{(n+\frac{1}{2})}+\dfrac{(n+2)^2}{(2n+1)(2n+3)(n+\frac{5}{2})}+\dfrac{(n+1)^2}{(2n+1)(2n+3)(n+\frac{1}{2})}-\dfrac{n(n+1)}{(n+\frac{1}{2})(2n-1)(2n+1)}\right], & m=n+1\\ \dfrac{n(n+1)(n+2)(n+3)}{(n+\frac{1}{2})(2n+3)(2n+5)(2n+7)}, & m=n+3\\ 2-\dfrac{n(n+1)(n-1)(n-2)}{(n+\frac{1}{2})(2n-1)(2n-3)(2n-5)}, & m=n-3\\ 1-(-1)^{n+m}, & m<n-1 \text{ and } m\neq n-3\\ 0, & \text{otherwise}\end{cases}$$

$$C8(m,n) = \begin{cases} \dfrac{2(n+1)(n+2)(n+3)}{(2n+1)(2n+3)(2n+5)(2n+7)}, & m = n+3 \\ \dfrac{2(n+1)(n+2)^2}{(2n+1)(2n+3)^2(2n+5)} + \dfrac{2(n+1)}{(2n+3)}\left[\dfrac{(n+1)^2}{(2n+1)^2(2n+3)} + \dfrac{n^2}{(2n+1)^2(2n-1)}\right], & m = n+1 \\ \dfrac{2n(n-1)^2}{(2n+1)(2n-1)^2(2n-3)} + \dfrac{2n}{(2n-1)}\left[\dfrac{(n+1)^2}{(2n+1)^2(2n+3)} + \dfrac{n^2}{(2n+1)^2(2n-1)}\right], & m = n-1 \\ \dfrac{2n(n-1)(n-2)}{(2n+1)(2n-1)(2n-3)(2n-5)}, & m = n-3 \\ 0, \quad \text{otherwise} \end{cases}$$

STABILITE DE LA CONVECTION NATURELLE DANS UN ESPACE ANNULAIRE SPHERIQUE ETROIT POUR DES PERTURBATIONS AXISYMETRIQUES

Résumé—On étudie la stabilité linéaire pour des perturbations axisymétriques de la convection naturelle dans un espace étroit entre deux sphères concentriques. On cherche la solution de perturbation avec le paramètre $\varepsilon = 1-\eta$, où η est le rapport des rayons interne et externe, en allant jusqu'à l'ordre huit. Les équations sont réduites à un système d'équations différentielles à l'aide d'une méthode de développements partiels spectraux. Ces équations constituent un problème de valeurs propres qui est résolu pour un nombre de Rayleigh fonction de η et pour nombre de Prandtl Pr. Les cas considérés sont $Pr = 0{,}1$, 1, 10 et 100 pour $0{,}900 \leqq \eta \leqq 0{,}995$. Une comparaison avec les résultats expérimentaux trouvés dans la littérature indique que la bifurcation non axisymétrique périodique dans le temps prend le dessus sur le cas considéré pour $Pr = 1$, 10. Néanmoins il apparaît que la bifurcation stable axisymétrique est possible pour $Pr = 0{,}1$.

DIE STABILITÄT DER NATÜRLICHEN KONVEKTION IM SCHMALEN KUGELFÖRMIGEN RINGSPALT

Zusammenfassung—Die lineare Stabilität im Hinblick auf achsensymmetrische Störungen der natürlichen Konvektion im schmalen Spalt zwischen Kugelschalen wird untersucht. Die Grundbewegung wird aus einem Störungsansatz 8. Ordnung für den Parameter $\varepsilon = 1-\eta$ ermittelt, wobei η das Verhältnis von Innenradius zu Außenradius des Ringes ist. Die Störungsgleichungen werden auf ein System von gewöhnlichen Differentialgleichungen mittels einer Methode der partiellen Spektralentwicklungen zurückgeführt. Diese Gleichungen bilden ein Eigenwertproblem, welches für die kritische Rayleigh-Zahl als eine Funktion von η und der Prandtl-Zahl Pr gelöst wird. Betrachtet wurden die Fälle mit $Pr = 0{,}1$, 1, 10 und 100 für $0{,}9 \leqslant \eta \leqslant 0{,}995$. Ein Vergleich mit den experimentellen Ergebnissen aus der Literatur zeigt, daß die nicht achsensymmetrische, zeitlich periodische Eingabelung sehr wahrscheinlich gegenüber dem hier betrachteten Fall mit $Pr = 1$ und 10 vorzuziehen ist. Es zeigt sich jedoch, daß die stationäre achsensymmetrische Eingabelung für $Pr = 0{,}1$ möglich ist.

УСТОЙЧИВОСТЬ ЕСТЕСТВЕННОЙ КОНВЕКЦИИ В УЗКОМ ЗАЗОРЕ МЕЖДУ ДВУМЯ СФЕРАМИ

Аннотация—Исследуется линейная устойчивость по отношению к осесимметричным возмущениям естественной конвекции в узком зазоре между двумя сферами. Основное решение представлено в рамках теории возмущений восьмого порядка по малому параметру $\varepsilon = 1-\eta$, где η—отношение внутреннего радиуса канала к наружному. Уравнения для возмущений приводятся к системе обыкновенных дифференциальных уравнений с помощью метода спектральных разложений. Эти уравнения описывают задачу на собственные значения, которая решается для критического числа Рэлея в зависимости от параметра η и числа Прандтля, Pr. Рассматриваются случаи, когда $Pr = 0{,}1$, 1, 10 и 100 при $0{,}900 < \eta < 0{,}995$. Сравнение с имеющимися в литературе экспериментальными данными показывает, что неосесимметричная периодическая бифуркация будет, вероятно, превалировать над рассматриваемым случаем при $Pr = 1$ и $Pr = 10$. Вероятно, стационарная осесимметричная бифуркация возможна при $Pr = 0{,}1$.